Optical and Magnetic Properties of Iron(II)–Nitrosyl Complexes in Model Compounds†

Jaqui A. Farrar, Roger Grinter, Dean L. Pountney and Andrew J. Thomson*
Centre for Metalloprotein Spectroscopy and Biology, School of Chemical Sciences, University of East Anglia, Norwich NR4 7TJ, UK

The iron(II) nitrosyl complexes [FeL(NO)] (L = ethylenediamine-, ethylenedioxydiethylenedinitrilo- or 1,6-diaminohexane-*N,N,N',N'*-tetraacetate) have been studied by absorption, low-temperature magnetic circular dichroism (MCD) and EPR spectroscopies. All three complexes exhibit similar spectral properties. The EPR spectra can be understood in terms of an axial site with a $S = \frac{3}{2}$ electronic ground state. Analysis of the optical spectra has been carried out following extended-Hückel molecular orbital calculations on $[Fe(H_2O)_5(NO)]^{2+}$ assuming C_{4v} symmetry for the iron(II) ion with the Fe–NO bond providing the major axis of distortion. Thus it has been possible to identify and assign the MCD transitions within the Fe–NO fragment of the complexes. This analysis provides a basis for understanding and interpreting the magneto-optical spectra of the nitrosyl complexes of iron(II) sites in non-haem iron proteins.

Nitric oxide (NO) will react with a variety of transition-metal compounds to form nitrosyl complexes. It will bind to metal ions in enzymes which react with dioxygen and is thus a useful probe of dioxygen binding sites. Since nitric oxide is an odd-electron molecule it has been used extensively as a spin label of the high-spin iron(II) sites of non-haem iron-containing enzymes such as lipoxygenase,[1] putidamonoxin[2] and isopenicillin N synthetase.[3] In such enzymes addition of the odd electron, $S = \frac{1}{2}$, NO species to a high-spin, $S = 2$, iron(II) site results in an EPR-active, $S = \frac{3}{2}$, species. There are two reports[4] of the use of NO to label a binuclear iron site in proteins to generate a $S = \frac{1}{2}$ species namely haemerythrin and the ferroxidase centre of bacterioferritin.

Nitric oxide also reacts readily with high-spin iron(II) ions in ferro-haemoproteins such as myoglobin, haemoglobin and cytochrome oxidase to generate low-spin Fe^{II}, d^6. The odd electron added by NO gives rise to an EPR signal at $g \approx 2.0$ which invariably displays not only the ^{14}N ($I_N = 1$) hyperfine coupling of NO itself but also transferred hyperfine from the in-plane N atom of the tetrapyrrole ring and of the ligand *trans* to the NO if that is also nitrogen.[5,6] Nitric oxide has also been shown to bind to the high-spin iron(III) state of haem, causing the latter to switch low spin, $S = \frac{1}{2}$, and, as a result of coupling to the odd electron of the NO molecule, form a diamagnetic state.[7]

These applications of nitric oxide as a spin label of the reactive sites in proteins has been given added interest by the recent discovery that NO itself is a novel class of intercellular signalling agent which causes smooth muscle to relax[8] and can act as a neurotransmitter at synapses.[9] The generation of NO *in vivo* is from L-arginine which is oxidised to L-citrulline (N^5-carbomoylornithine) and NO by an enzyme, NO synthase,[10] closely related to P-450. The detector of NO in these signalling processes is thought to be the haem group of soluble guanylate cyclase.[11]

The use of NO as a probe of non-haem iron(II) sites in enzymes has so far concentrated on the use of EPR spectroscopy. In this laboratory we have undertaken the study of a number of non-haem iron proteins by means of both EPR and low-temperature MCD (magnetic circular dichroism) spectroscopies. To facilitate understanding of the nature of the active site extensive use has been made of nitric oxide derivatives of these proteins. However in order to allow us to make a fuller interpretation of the spectroscopic results a number of simple iron(II) model systems have also been employed. It is these complexes of nitric oxide that are discussed in this paper.

† *Non-SI units employed:* eV $\approx 1.60 \times 10^{-19}$ J, G = 10^{-4} T.

Results

Three models have been studied in this work, namely the complexes [Fe(edta)(NO)] (H_4edta = ethylenediamine-*N,N,N',N'*-tetraacetic acid), [Fe(egta)(NO)] {H_4egta = ethylenedioxydiethylenedinitrilotetraacetic acid [ethylene glycol bis(2-aminoethyl ether)-*N,N,N',N'*-tetraacetic acid]} and [Fe(hdta)(NO)] (H_4hdta = 1,6-diaminohexane-*N,N,N',N'*-tetraacetic acid).

The low-temperature EPR spectra of the three nitric oxide complexes are shown in Fig. 1. The observed g values can be understood in terms of a $S = \frac{3}{2}$ ground-state spin system and the spin Hamiltonian (1), where the symbols have their

$$\mathcal{H} = g_0B_0S + D[S_z^2 - \tfrac{1}{3}S(S+1)] + E(S_x^2 - S_y^2) \quad (1)$$

conventional meanings. The $S = \frac{3}{2}$ state is subject to a zero-field distortion which separates two effective spin doublets, $M_S = \pm\frac{1}{2}$ and $\pm\frac{3}{2}$, by $2D$. In the case of an axial system, where $E = 0$, and when $D > g_0B_0S$, the $M_S = \pm\frac{1}{2}$ doublet is lower in energy with effective g values $g_\perp = 4$ and $g_\parallel = 2$. The upper doublet, $M_S = \pm\frac{3}{2}$, has effective g values of $g_\parallel = 6$ and $g_\perp = 0$. However the transition intensity within it will be zero. Increasing the rhombicity, $E > 0$, splits the ground-stage $g_\perp = 4$ signal. In a system of maximum rhombicity, $E/D = 0.33$, signals are obtained at $g = 5.45$, 2.02 and 1.47. The signals observed in the case of the nitrosyl compounds have $g_\perp$ close to 4. Hence the lower doublet is $M_S = \pm\frac{1}{2}$, D must be positive and E is small. No signals have been detected from the upper doublet. The g values of the signals observed from the lowest doublet and those calculated for both Kramers doublets using $g_0 = 2.0$ and appropriate E/D values are presented in Table 1 for each of the complexes.

The room-temperature ultraviolet–visible region absorption spectra of all three complexes are shown in Fig. 2 and details of the spectra are given in Table 2. The complexes exhibit similar optical spectra with three broad transitions at wavelengths longer than 300 nm, at around 350, 440 and 620 nm. The

Table 1 Observed and calculated g values for the NO complexes

Complex		g values Observed			Calculated*			E/D
[Fe(edta)(NO)]	$\|\pm 1/2\rangle$	4.1	3.95	2.01	4.07	3.93	1.999	0.012
	$\|\pm 3/2\rangle$				0.07	0.07	5.999	
[Fe(hdta)(NO)]	$\|\pm 1/2\rangle$	4.09	3.96	1.99	4.07	3.93	1.999	0.012
	$\|\pm 3/2\rangle$				0.07	0.07	5.999	
[Fe(egta)(NO)]	$\|\pm 1/2\rangle$	4.06	3.97	1.99	4.07	3.93	1.999	0.012
	$\|\pm 3/2\rangle$				0.07	0.07	5.999	

* Calculated according to the spin Hamiltonian (1) with $g_0 = 2.00$ and $D = 5\ cm^{-1}$.

Table 2 Summary of the optical spectral data

Complex	Room-temperature absorbance λ/nm(ε/dm^3 mol^{-1} cm^{-1})	MCD at 4.2 K and 5 T λ/nm($\Delta\varepsilon$/dm^3 mol^{-1} cm^{-1})
[Fe(edta)(NO)]	340 (570)	330 (22)
	435 (436)	440 (35)
		515 (sh) (10)
	630 (79.5)	660 (8)
		760 (sh) (5)
[Fe(hdta)(NO)]	n.m.*	298 (58)
	334 (sh) (607)	340 (sh) (30)
	443 (303)	445 (22)
	600 (73.5)	625 (5)
		760 (3)
[Fe(egta)(NO)]	350 (sh) (1034)	345 (42)
	434 (302)	445 (15)
	620 (70)	660 (3)

* Not measured.

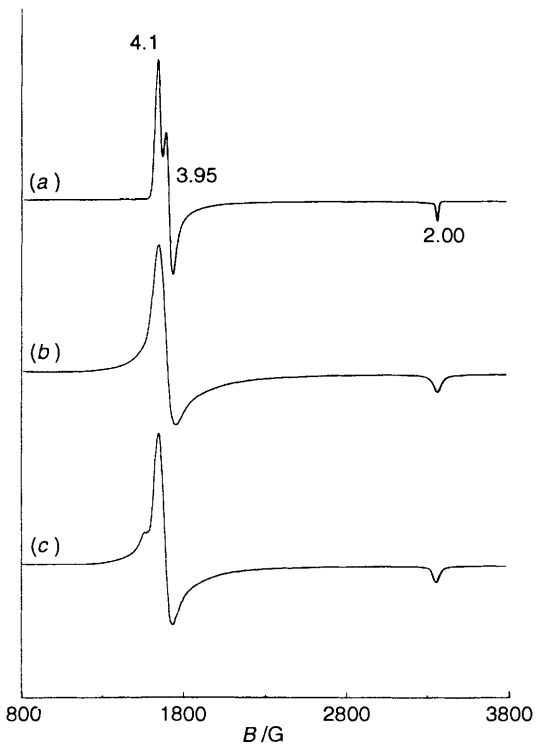

Fig. 1 The EPR spectra of the iron(II) nitrosyl complexes in the presence of ethane-1,2-diol: (*a*) [Fe(edta)(NO)], (*b*) [Fe(hdta)(NO)], (*c*) [Fe(egta)(NO)]. Measurement conditions: $T = 5$ K, $P = 2.03$ mW, $\nu = 9.42$ GHz, modulation frequency = 100 kHz, modulation amplitude = 8 G

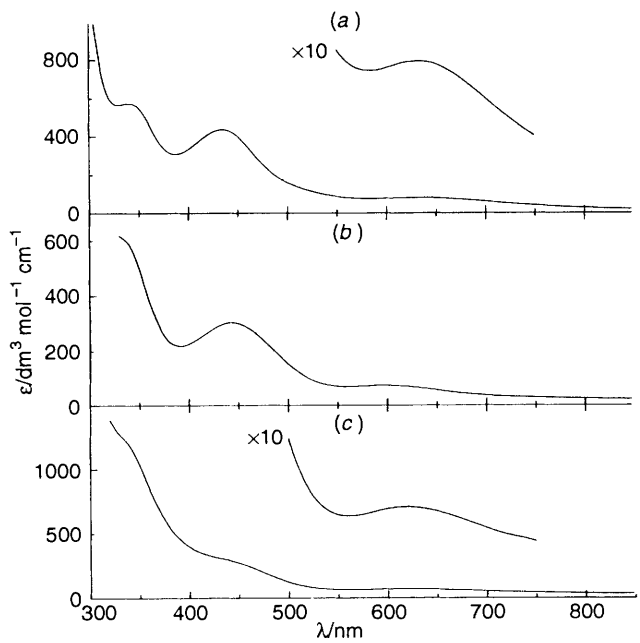

Fig. 2 Room-temperature optical spectra in the presence of ethane-1,2-diol of (*a*) [Fe(edta)(NO)], (*b*) [Fe(hdta)(NO)], (*c*) [Fe(egta)(NO)]

resolution of these bands differs for each complex. Addition of ethane-1,2-diol to 50% (v/v) had no effect on the optical spectra (data not shown).

The low-temperature MCD spectra of each of the complexes in a 50% (v/v) mixture of ethane-1,2-diol are presented in Figs. 3(*a*), 4(*a*) and 5(*a*). The MCD spectrum of [Fe(edta)(NO)] was measured to 2000 nm and no additional bands were detected. The MCD spectra show bands of only one sign. The field dependence at a fixed temperature of 1.6 K is shown for the band at 440 nm of each complex, Figs. 3(*b*), 4(*b*) and 5(*b*). In addition, the temperature dependences of the bands have been measured. These curves, presented for the band at 440 nm of each complex in Figs. 3(*c*), 4(*c*) and 5(*c*), show the temperature

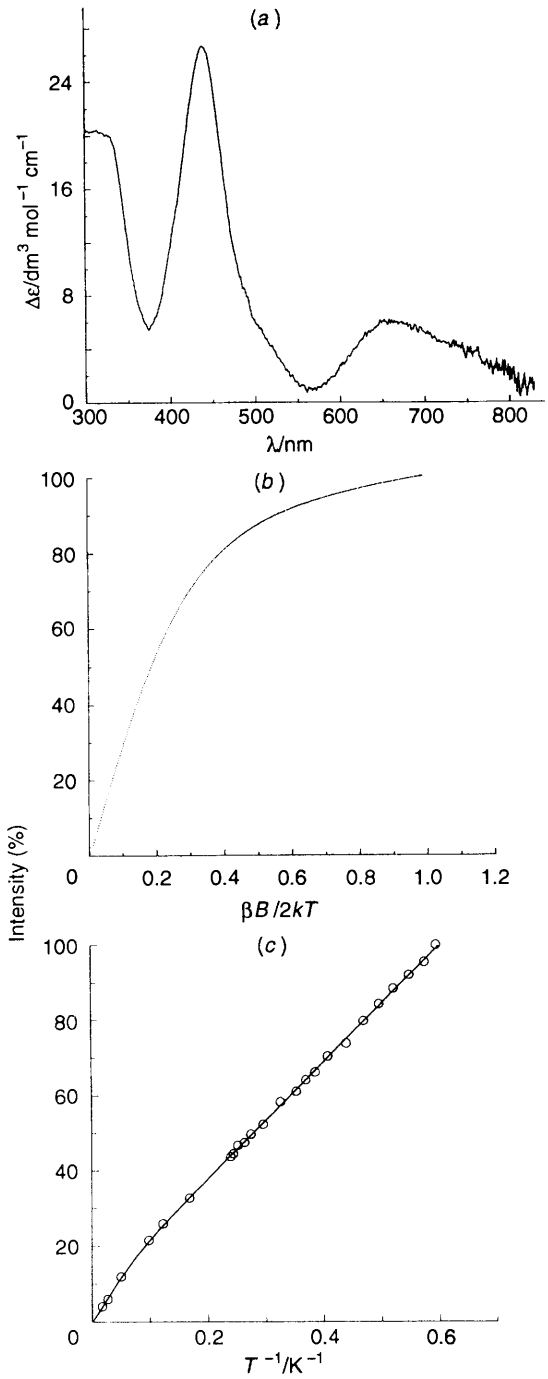

Fig. 3 The MCD data for [Fe(edta)(NO)]: (*a*) spectrum at 4.2 K from 300 to 850 nm; (*b*) magnetisation curve at 1.6 K and 440 nm; (*c*) $1/T$ plot at 440 nm (○), with best-fit simulation (——). Details of the simulation parameters are given in Table 3

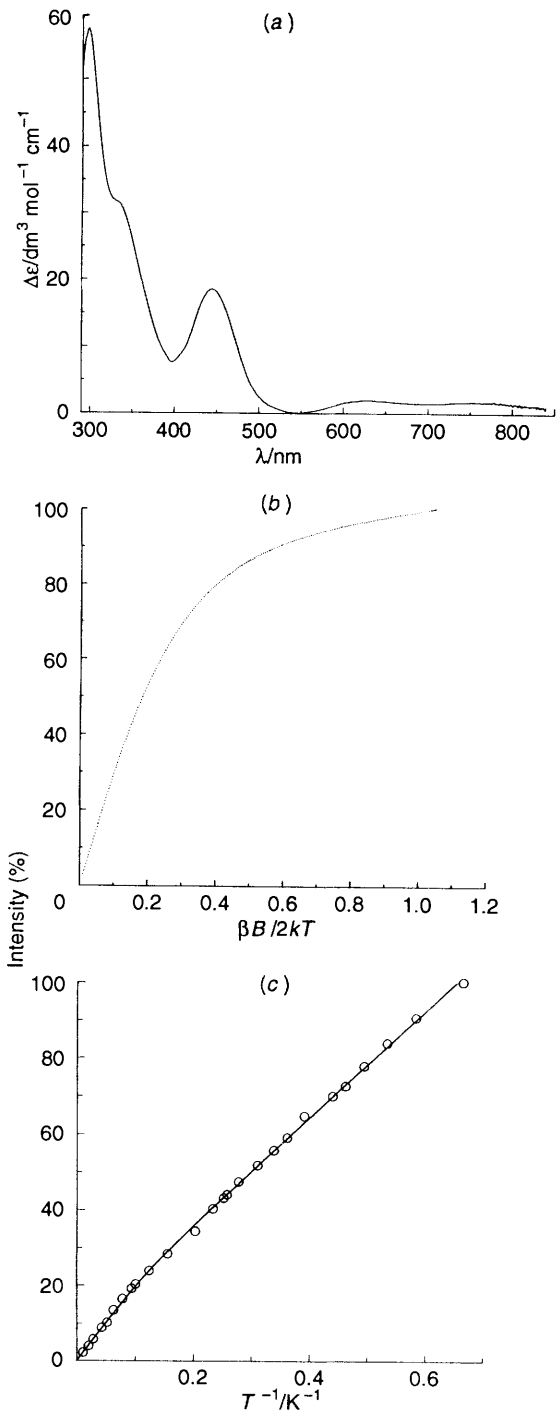

Fig. 4 The MCD data for [Fe(hdta)(NO)]: (*a*) spectrum at 4.2 K from 290 to 850 nm; (*b*) magnetisation curve at 1.6 K and 445 nm; (*c*) $1/T$ plot at 445 nm (○), together with best-fit simulation (——). Details of the simulation parameters are given in Table 3

dependence of the bands at magnetic fields of 0.4 T, where the signal intensity is proportional to the applied field.[12] Details of the band positions and intensities are given in Table 2.

The non-linear nature of the plot of MCD intensity against $1/T$ gives direct evidence for the thermal population of the higher Kramers doublet of the $S = \frac{3}{2}$ ground state. The zero-field splitting, D, can be estimated from the data as follows. The intensity, I, of the MCD spectrum for a $S = \frac{3}{2}$ system at any wavelength is given by equation (2) where K contains a set of

$$I = K\{[(C_1/kT) + B_1 + A_1]\alpha_1 + [(C_2/kT) + B_2 + A_2]\alpha_2\} \quad (2)$$

parameters including the magnetic field, the sample concentration and pathlength;[12] $A_{1,2}$, $B_{1,2}$ and $C_{1,2}$ are the A, B and C terms for the lower and upper Kramers doublets respectively. The MCD intensity for each doublet is given by the A, B and C terms for that doublet, which are dependent upon the ground- and excited-state Zeeman splitting, the field-induced mixing of the upper and lower doublet and any second-order Zeeman mixing with higher-lying states.[12–14] The parameters α_1 and α_2 are the fractional populations of the two zero-field levels and are given by equations (3a) and (3b) where $2D$ is the zero-field

$$\alpha_2 = \frac{e^{-2D/kT}}{(1 + e^{-2D/kT})} \quad (3a)$$

$$\alpha_1 = 1 - \alpha_2 \quad (3b)$$

splitting of the two Kramers doublets. Equation (2) is only valid in the limit where the MCD spectrum is linearly dependent upon the magnetic field. Hence the data were collected under these conditions.

Figs. 3(*c*), 4(*c*) and 5(*c*) give the experimental data together with the best-fit simulations for a selected band from each of [Fe(edta)(NO)], [Fe(hdta)(NO)] and [Fe(egta)(NO)] respectively. The high-temperature slope in each case passes through the origin showing the contribution of A terms and out-of-state B terms to be negligible. Therefore A_1 and A_2 have been set to zero. The B terms between the upper and lower (B_2) and lower and upper (B_1) Kramers doublets are equal to one another but opposite in sign. Hence B_1 was set equal to $-B_2$. For each complex a D value was sought that was the same within experimental error for each of the curves constructed while the parameters B_2, C_1 and C_2 were allowed to vary freely to minimise the value of χ^2. The values of the simulation parameters required to fit each of the $1/T$ curves constructed are presented in Table 3.

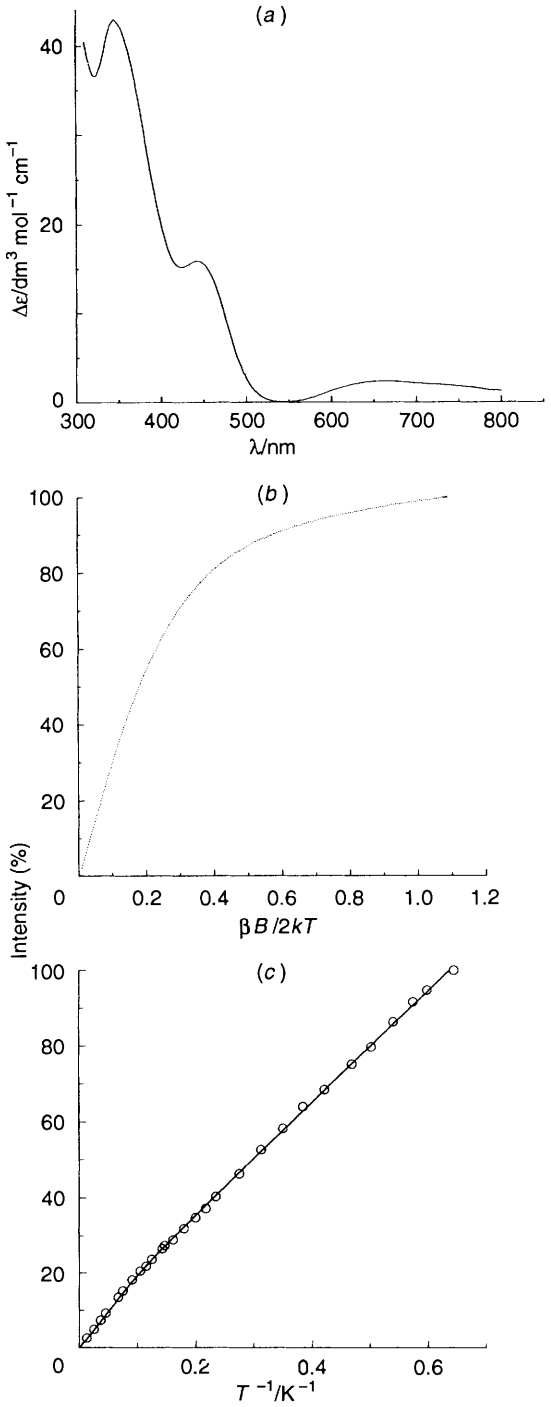

Fig. 5 The MCD data for [Fe(egta)(NO)]: (*a*) spectrum at 4.2 K from 310 to 800 nm; (*b*) magnetisation curve at 1.6 K and 445 nm; (*c*) $1/T$ plot at 445 nm (○), together with best-fit simulation (——). Details of the simulation parameters are given in Table 3

Interpretation

In order to arrive at an assignment of the optical spectra of the nitrosyl complexes it is necessary to establish the orbital nature of the electronic ground state and to use an energy-level scheme for the excited states.

The starting point for our analysis of the Fe–NO transitions is the detailed molecular orbital calculations in C_{4v} symmetry by Fenske and DeKock[15] and Enemark and Feltham.[16] The energy levels of a transition-metal nitrosyl complex are more conveniently described in terms of the molecular orbitals of the triatomic fragment M–N–O which are subject to a local crystal field generated by the other ligands around the metal. Taking M–N–O to be linear and assuming a C_{4v} field, a reasonable molecular orbital (MO) energy-level scheme has been derived based on this analysis, Scheme 1. Molecular orbital formation

Table 3 Summary of the parameters obtained from fitting of the temperature dependence of the MCD bands in the linear-field limit

Complex	λ/nm	$2D$/cm^{-1}	$B_1(=-B_2)$	C_1	C_2
[Fe(edta)(NO)]	440	22 ± 3	−6.4	100	1
[Fe(hdta)(NO)]	298	15 ± 3	−1.5	100	100
	445	15 ± 3	−8.4	100	100
[Fe(egta)(NO)]	345	15 ± 3	4.1	100	130
	445	15 ± 3	−6.1	100	20
	660	15 ± 3	−14.6	100	100

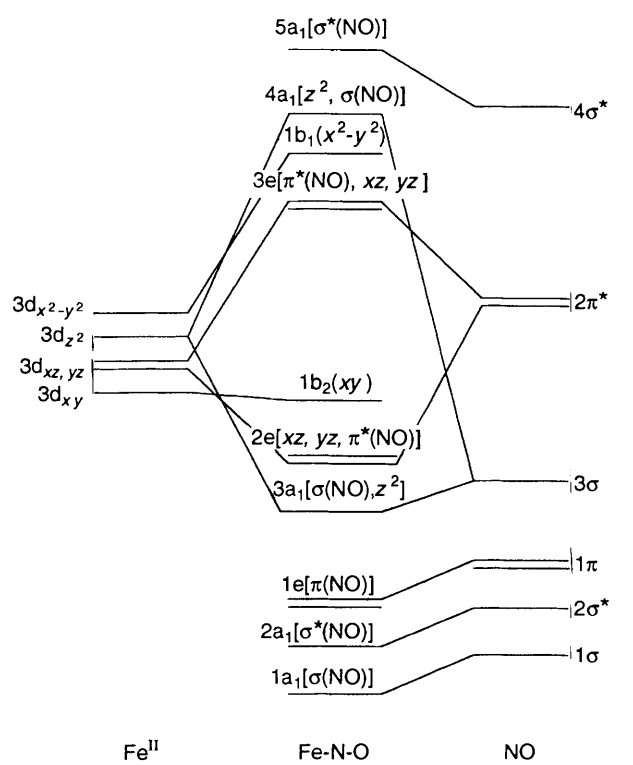

Scheme 1 Molecular orbital scheme derived for a linear Fe–NO fragment under C_{4v} symmetry, based on the calculations contained in refs. 15 and 16

in the fragment M–N–O is proposed to take place by overlap between the lone pair of the N atom, and the metal d_{z^2} orbital and by overlap between the π^* orbitals of NO and the $d_{xy,yz}$ orbitals.[15,16]

When M is Fe^{II} the fragment Fe^{II}–NO possesses 17 electrons, ignoring the nitrogen and oxygen 1 s electrons as part of the core shell. Two possible ground-state configurations can be considered, namely a low-spin form $(1a_1)^2(2a_1)^2(1e)^4(3a_1)^2(2e)^4(1b_2)^2(3e)^1$ and a high-spin form $(1a_1)^2(2a_1)^2(1e)^4(3a_1)^2(2e)^4(1b_2)^1(3e)^2$. The low-spin configuration gives rise to only one electronic ground state, ^2E, with $S = \frac{1}{2}$ and an orbital degeneracy. The high-spin configuration generates four spin doublets and one spin quartet, that is $^2A_1$, $^2A_2$, $^2B_1$, $^2B_2$ and $^4B_1$.

The EPR spectra of the nitrosyl complexes of Fe(edta), Fe(hdta) and Fe(egta), Fig. 1, suggest an electronic ground state with a spin $S = \frac{3}{2}$ and no first-order orbital momentum, $g_0 = 2.0$. Thus the ^2E state of the low-spin configuration does not accord with the experimental results. The ^2E state will have a first-order orbital moment given by the contribution of the metal $d_{xz,yz}$ orbitals to the 3e MO. Spin–orbit coupling will therefore split the ^2E state into a pair of Kramers doublets, classified as E′ and E″ under the double group of C_{4v}. The doublets correspond to pairs of components with M_J values of $\pm\frac{3}{2}$ and $\pm\frac{1}{2}$. In the $|M_S, M_L\rangle$ representation the wavefunction can be written as $|M_J \pm \frac{3}{2}\rangle = |\pm\frac{1}{2}, \pm 1\rangle$ and $|M_J \pm \frac{1}{2}\rangle = |\mp\frac{1}{2}, \pm 1\rangle$. The doublet $M_J = \pm\frac{1}{2}$ will undergo no first-order splitting so that $g_{\|} = g_{\perp} = 0.0$. Hence, we rule out the low-spin configuration.

The states of the high-spin configuration are all orbital singlets and hence have no first-order orbital momentum. The spin doublets will all give g values close to 2.0, the spin-only value. However, the quartet state, $^4B_1$, will split under the influence of second-order spin–orbit coupling and an axial distortion field into pairs of Kramers doublets. The g values can be described in terms of the effective spin formalism using a spin Hamiltonian (1). These values accord with the observed g values for the Fe–NO complexes studied, where the signals have been assigned to transitions within the $M_S \pm \frac{1}{2}$ Kramers doublet with a slight rhombicity ($E/D \neq 0$), see Fig. 1 and Table 1. Thus the experimental EPR evidence strongly favours the assignment of the ground state as the $^4B_1$ state of the high-spin configuration $(1b_2)^1(3e)^2$.

The low- and high-spin configurations are expected to have different M–N–O bond angles. The low-spin configuration has one electron in the 3e orbital. Bending of the bond angle away from 180° would lead to a lifting of the 3e orbital degeneracy and result in a nett stabilisation of the electron. Hence this configuration is predicted to distort. On the other hand the high-spin configuration places two electrons in the 3e orbital and no nett stabilisation will take place as the M–N–O bond is bent. Fitting of the observed g values by the spin Hamiltonian (1) shows a very small rhombic splitting of g_{xy} for all three complexes studied, see Table 1. This suggests that these complexes have a ground-state symmetry very close to C_{4v}, consistent with an almost linear Fe–N–O unit and also with the Fe–N–O bond providing the major axial distortion axis.

Having established that the ground state is $^4B_1$, we turn to the assignment of the optical transitions detected. Magneto-optical spectra for the three complexes in the absence of nitric oxide have been studied. The MCD spectrum of the Fe(egta) complex at 4.2 K is shown in Fig. 6 and similar spectra were obtained for the Fe(edta) and Fe(hdta) complexes. Intense transitions are observed below 400 nm. These bands are tentatively assigned to O or N to Fe charge-transfer transitions. However there are no ligand-to-metal charge-transfer transitions in the visible region of the electronic spectrum. Thus by comparison with the nitrosyl-free complexes the bands between 400 and 850 nm can be ascribed to transitions within the Fe–NO fragment of the nitrosyl complexes. An MO calculation, to be described below, shows that a substantial transition dipole moment may be

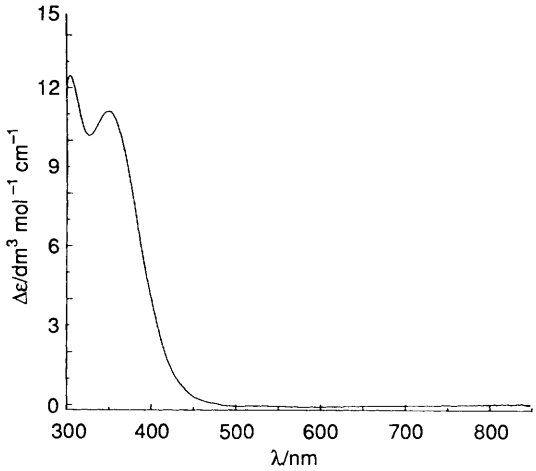

Fig. 6 The MCD spectrum of [Fe(egta)] at 4.2 K from 300 to 850 nm

obtained for transitions between two π and two π^* MOs formed from the $3d_{xz}$ and $3d_{yz}$ atomic orbitals (AOs) of the iron and the $2p_x$ and $2p_y$ AOs of the nitrogen and oxygen.

Table 4 shows possible one-electron transitions for the energy levels depicted in Scheme 1, together with the linear polarisations for those transitions under the point group C_{4v}. The transitions are polarised either along the Fe–N–O axis, z, or perpendicular to this axis, xy. The latter transitions are expected to be to an excited E state with an orbital degeneracy. The MCD transitions to spin–orbit components of a ^4E excited state will give rise to C terms of opposite sign. The MCD spectra of the nitrosyl derivatives at 4.2 K, see Figs. 3(*a*), 4(*a*) and 5(*a*), are dominated by the C-term contribution and only show C terms of one sign. This suggests that the optical transitions are polarised principally along the Fe–N–O axis. The field dependence of the MCD bands at 1.6 K gives support to this analysis. The g values of the lowest Kramers doublet of the ground state are highly anisotropic with $g_z = 2.0$ and $g_{xy} = 4.0$. Optical transitions which are xy polarised will select only molecules with molecular z axes parallel to the magnetic field. The magnetisation curve (field dependence)[17,18] will reflect a ground state g value of 2.0 and give an intercept of 0.5. However, an optical transition with predominantly z polarisation will select molecules with either the x or y axis parallel to the magnetic field and hence will give a magnetisation curve typical of ground-state Zeeman splitting characterised by $g = 4.0$. An intercept value, I, of 0.278 will be obtained.[18] The steep magnetisation curves shown for all the optical transitions are consistent with optical transitions which are primarily z-axis polarised. The polarisation cannot however be purely along z since the MCD C terms would then be zero. It is necessary to have some component of the optical transition perpendicular to the z axis.

An energy-level scheme has been derived using an extended-Hückel molecular orbital (EHMO) approximation[19] using the parameters in Table 5. The H_{ij} values were calculated by means of the modified Wolfsberg–Helmholtz approximation.[20] The ion $[Fe(H_2O)_5(NO)]^{2+}$ was chosen as the basis molecule for the calculation as it qualitatively takes account of the ligands whilst still keeping the total number of atoms to a manageable size. The bond lengths used were N–O 1.15, Fe–N 1.63 and Fe–O 2.00 Å. The atomic orbitals included were the H 1s, O 2s and 2p, N 2s and 2p and Fe 4s, 4p and 3d. The Fe–N–O bond angle was set at 180°. The point group is C_{4v} if only atoms in the first co-ordination sphere are taken into account. The resulting molecular orbital scheme, together with the form of the 2e and 3e molecular orbitals, is shown in Scheme 2, (*a*) and (*b*). The relative contribution of each atomic orbital, Fe $3d_{xz,yz}$, N $2p_{x,y}$ and O $2p_{x,y}$, to the resulting molecular orbital is shown by the size of that orbital in Scheme 2(*a*), and the representation is not

Table 4 Possible one-electron transitions within a linear Fe–N–O fragment under C_{4v} symmetry

One-electron transition	Excited configuration[a]	Excited-state polarisation[b]	
$3e \longrightarrow 1b_1$[c]	$(1b_2)^1(3e)^1(1b_1)^1$	^4E	XY
$3e \longrightarrow 4a_1$	$(1b_2)^1(3e)^1(4a_1)^1$	^4E	XY
$3e \longrightarrow 5a_1$	$(1b_2)^1(3e)^1(5a_1)^1$	^4E	XY
$1b_2 \longrightarrow 3e$	$(3e)^3$	^2E (spin forbidden)	XY
$1b_2 \longrightarrow 1b_1$	$(3e)^2(1b_1)^1$	$^4B_2$	F[d]
$1b_2 \longrightarrow 4a_1$	$(3e)^2(4b_1)^1$	$^4A_2$	F
$1b_2 \longrightarrow 5a_1$	$(3e)^2(5a_1)^1$	$^4A_2$	F
$2e \longrightarrow 1b_2$	$(2e)^3(1b_2)^2(3e)^2$	^4E	XY
$2e \longrightarrow 3e$	$(2e)^3(1b_2)^1(3e)^3$	$^4B_1$ (plus others)	Z
$2e \longrightarrow 1b_1$	$(2e)^3(1b_2)^1(3e)^2(1b_1)^1$	^4E	XY
$2e \longrightarrow 4a_1$	$(2e)^3(1b_2)^1(3e)^2(4a_1)^1$	^4E	XY
$3a_1 \longrightarrow 1b_2$	$(3a_1)^1(3e)^2$	$^4A_2$	F
$3a_1 \longrightarrow 3e$	$(3a_1)^1(1b_2)^1(3e)^3$	^4E	XY
$3a_1 \longrightarrow 1b_1$	$(3a_1)^1(1b_2)^1(3e)^2(1b_1)^1$	$^4A_2$	F
$3a_1 \longrightarrow 4a_1$	$(3a_1)^1(1b_2)^1(3e)^2(4b_1)^1$	$^4B_1$	Z

[a] From a high-spin ground-state electron configuration, $(1b_2)^1(3e)^2$. [b] From a $^4B_1$ ground state. [c] Orbitals are as in Schemes 1 and 2. [d] F = forbidden transition.

Table 5 Parameters used in the extended-Hückel calculations

Orbital	H_{ii}/eV	ζ_1
Fe 3d*	−12.60	5.35
Fe 4p	−5.32	1.90
Fe 4s	−9.10	1.90
O 2p	−14.80	2.28
O 2s	−32.30	2.28
N 2p	−13.4	1.95
N 2s	−26.00	1.95
H 1s	−13.60	1.30

* $\zeta_2 = 2.00$, coefficients in the double-ζ expansion are $c_1 = 0.5505$ and $c_2 = 0.6260$.

intended to show the overlap of the AOs. Scheme 2(*b*) shows considerable agreement with the qualitative scheme, Scheme 1, based on the analyses presented in refs. 15 and 16. However the energies and form of the molecular orbitals given by the EHMO calculation allow assignment of visible-region transitions. Although care has to be exercised in applying the results of this EHMO calculation to the interpretation of the observed electronic spectra, there are few potential one-electron transitions in the energy region of interest. The $1a_2$ and 1e molecular orbitals lie at around −15 eV ($\approx$12 100 cm^{-1}) and have negligible contributions from the atomic orbitals of Fe or NO, and so transitions involving these MOs are disregarded. Additional MOs having small coefficients for the AOs of Fe and NO lie just below the $1a_2$ and 1e MOs. We disregard these also on the grounds of both energy gap and insignificant AO coefficients. Transitions to the empty $4a_1$ molecular orbital are too high in energy to be observed in the visible or near-UV region and again this orbital is disregarded.

The five remaining molecular orbitals, 2e, $1b_2$ and 3e, have similar energies and are relatively isolated from the others. Of these the most intense band(s) should be associated with the 2e to 3e transition. The $1b_2$ orbital is essentially the iron d_{xy} orbital with no contribution from the NO and very little from the other ligands. Any transitions involving it and the 2e or 3e orbitals will therefore effectively be d–d transitions and might be expected to be weak. From a $^4B_1$ ground state only transitions to a $^4B_1$ excited state are allowed in z polarisation. Thus for a Fe–N–O bond angle of 180° the energy-level scheme suggests one intense transition, in the visible region of the spectrum, Scheme 2(*b*).

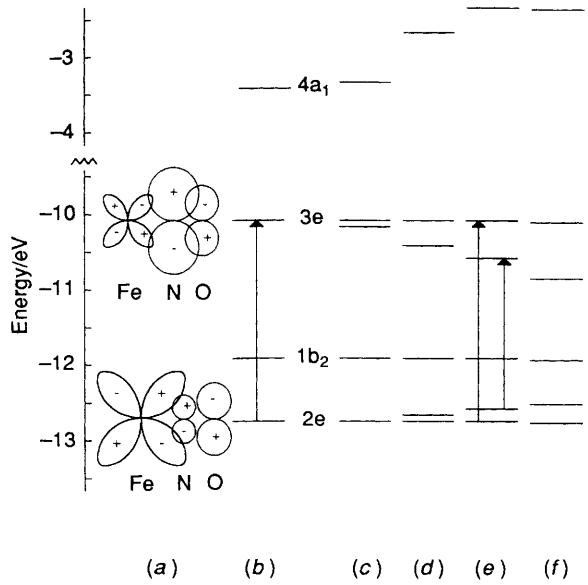

Scheme 2 Molecular orbital scheme resulting from EHMO calculations on $[Fe(H_2O)_5(NO)]^{2+}$: (*a*) representation of the 2e and 3e molecular orbitals given in terms of the major contributing atomic orbitals, $3d_{xy,yz}$, from the Fe and π^* from the NO; the contribution of each atomic orbital is governed by the atomic orbital coefficients taken from the text; (*b*) angle Fe–N–O 180°; (*c*) Fe–N–O 170°; (*d*) Fe–N–O 155°; (*e*) Fe–N–O 148°, (*f*) Fe–N–O 140°. Vertical arrows in (*b*) and (*e*) represent electronic transitions

The effect of varying the Fe–N–O bond angle has been investigated, considering only the MOs in the energy region of interest. The results of these EHMO calculations are presented in Scheme 2(*c*)–(*f*). As the NO group bends away from the z axis there is a lifting of the degeneracy of the 2e and 3e MOs to differing extents. As a result, one of the 2e ⟶ 3e transitions remains almost unchanged in energy while the energy of the other is considerably reduced. The two 2e ⟶ 3e z-polarised transitions, degenerate for an Fe–N–O angle of 180°, are thus separated in energy, Scheme 2(*e*). We therefore propose that they are responsible for the bands observed at around 440 and 660 nm in the Fe–NO complexes studied here. Since the EHMO calculations were carried out using $[Fe(H_2O)_5(NO)]^{2+}$ as the basis molecule it is not possible to state the exact Fe–N–O angle for the actual complexes studied.

The atomic orbital coefficients for the 2e and 3e π and π^* MOs, for a Fe–N–O angle of 180°, are found to be +0.792, +0.345 and −0.475 and −0.592, +0.807 and −0.520 for Fe $3d_{xz}/3d_{yz}$, N $2p_x/2p_y$ and O $2p_x/2p_y$ respectively. These AO coefficients provide a substantial transition dipole moment, along the Fe–NO bond, for the 2e ⟶ 3e transition. Reduction of the Fe–N–O bond angle changes these figures very little.

Conclusion

We have utilised and developed the molecular orbital scheme for nitrosyl complexes proposed by earlier workers[15,16] to give an effective description of the bonding within Fe–NO complexes. Our scheme satisfactorily explains the observed $S = \frac{3}{2}$ EPR signals and accounts for the characteristic optical and MCD data. This method of analysing the bonding within non-haem iron(II) nitrosyl complexes contrasts with the approach adopted by Solomon and co-workers[21] who have published preliminary data on both [Fe(edta)(NO)] and nitrosyl derivatives of mononuclear iron proteins. However both methods result in the same electronic ground-state spin, $S = \frac{3}{2}$, although the details of the bonding description varies. The approach adopted in ref. 21 describes the bonding in terms of a high-spin ($S = \frac{5}{2}$) iron(III) ion antiferromagnetically coupled to NO^-

($S = 1$) to give a resultant $S = \frac{3}{2}$ ground state. This explanation of the bonding is not totally at variance with the MO approach described here. Placing 17 electrons within the MOs of Scheme 1 results in movement of electrons out of iron-based 3d orbitals into orbitals with considerable NO character, resulting in a ground state with a certain degree of Fe^{III}–NO^- character.

Experimental

In each case the ligand, egta, edta or hdta (Aldrich Chemical Co., supplied as the free acid or disodium salt) was dissolved in aqueous solution to a final concentration of 100 mmol dm^{-3} and the pH adjusted to 7.2. The oxygen was then removed by extensive bubbling with argon which was first scrubbed free of oxygen by passage over an oxygen-scavenging column (Gas Free Oxygen Filter, Chrompack). A known quantity of solid ammonium iron(II) sulfate (Aldrich, reagent grade) and the ligand solution were taken into a nitrogen-atmosphere glove-box operating at less than 2 ppm oxygen (Faircrest Engineering Limited) and the iron dissolved in the appropriate ligand solution, such that the final iron concentration was approximately 20 mmol dm^{-3}, and the ligand concentration approximately 100 mmol dm^{-3}. All subsequent manipulations of the iron solution were made in an anaerobic environment.

Each nitric oxide iron(II) complex was made on a simple argon/vacuum line designed to allow the atmosphere above an iron(II) solution to be exchanged for gaseous nitric oxide (Aldrich, 98.5%), followed by stirring of the solution to incorporate the NO into solution and then the excess of nitric oxide, as shown by the characteristic EPR signal at $g = 2$, to be removed from the atmosphere and solution by stirring under a flow or scrubbed argon. Nitric oxide complex formation was monitored optically and full complex formation occurred within 20 min of the introduction of the nitric oxide atmosphere.

The NO complex was then either loaded into a quartz EPR tube or anaerobic quartz cuvette (pathlength 1 mm) for spectroscopic measurements. For cryogenic optical spectroscopy the sample is required to form an optical glass down to 1.6 K. To this end a glassing agent, ethane-1,2-diol in this case, was added to the sample to a final concentration of 50% (v/v). The EPR and ambient-temperature optical spectra were measured for each of the complexes in the presence and absence of glassing agent to confirm that the iron(II)/nitric oxide site is unaffected by the ethane-1,2-diol (data not shown).

Low-temperature magnetic circular dichroism spectra were recorded either on a JASCO 500D CD spectropolarimeter interfaced to an IBM PC-AT for the region from 300 to 1000 nm or a laboratory-built[22] NIR-CD spectropolarimeter capable of measurements to 3000 nm. For measurements in the near-infrared region the sample was formed using D_2O and deuteriated ethane-1,2-diol as the glassing agent. The sample was mounted in a SM4 split-coil superconducting magnet (Oxford Instruments plc, Oxford) capable of generating a magnetic field of up to 5 T and varying the sample temperature from 1.6 to 150 K. The absorption coefficients ($\Delta\varepsilon = \varepsilon_L - \varepsilon_R$) for the MCD spectra are based on the iron(II) ion concentration and are not normalised for magnetic field. Simulation of the MCD tempetature-dependence data was accomplished using an iterative graph fitting routine[23] running in Microsoft Windows.

Room-temperature ultraviolet–visible absorption spectra were recorded on a Hitachi U3200 double-beam spectrophotometer. Intensities are quoted in terms of the absorption coefficient, ε ($dm^3\ mol^{-1}\ cm^{-1}$), based on the iron concentration. The EPR spectra were recorded on a Bruker ER200D X-band spectrometer fitted with an Oxford Instruments ESR-9 flow cryostat which enables spectra to be measured down to 4.2 K.

References

1 J. C. Salerno and J. N. Siedow, *Biochim. Biophys. Acta*, 1979, **579**, 246.
2 H. Twilfer, F.-H. Bernhardt and K. Gersonde, *Eur. J. Biochem.*, 1985, **147**, 171.
3 V. J. Chen, A. Morville, M. R. Harpel, C. A. Frolik, K. Surerus, E. Münck and J. D. Lipscomb, *J. Biol. Chem.*, 1989, **264**, 21677.
4 J. M. Nocek, D. M. Kurtz, jun., J. T. Sage, P. G. Debrunner, M. J. Maroney and L. Que, jun., *J. Am. Chem. Soc.*, 1985, **107**, 3382; N. E. LeBrun, M. R. Cheasman, A. J. Thomson, G. P. Moore, S. C. Andrews, J. R. Guest and P. M. Harrison, *FEBS Lett.*, 1993, **323**, 261.
5 H. Kon, *Biochim. Biophys. Acta*, 1975, **379**, 103.
6 A. W. Addison and J. J. Stephanos, *Biochemistry*, 1986, **25**, 4104.
7 M. K. Johnson, A. J. Thomson, T. E. Walsh, D. E. Barber and C. Greenwood, *Biochem. J.*, 1980, **189**, 285.
8 L. J. Ignarro, *Semin. Hematol.*, 1989, **26**, 63.
9 J. Garthwaite, *Trends Neurosci.*, 1991, **14**, 60.
10 S. Moncada, R. M. J. Palmer and E. A. Higgs, *Pharmacol. Rev.*, 1991, **43**, 109.
11 F. Murad, *J. Clin. Invest.*, 1986, **78**, 1.
12 A. D. Buckingham and P. J. Stephens, *Annu. Rev. Phys. Chem.*, 1966, **17**, 399.
13 P. N. Schatz and A. J. McCaffery, *Q. Rev. Chem. Soc.*, 1969, **23**, 552.
14 S. B. Piepho and P. N. Schatz, *Group Theory in Spectroscopy, with Applications to Magnetic Circular Dichroism*, Wiley, New York, 1983.
15 R. F. Fenske and R. L. DeKock, *Inorg. Chem.*, 1972, **11**, 437.
16 J. H. Enemark and R. D. Feltham, *Coord. Chem. Rev.*, 1974, **13**, 339.
17 A. J. Thomson and M. K. Johnson, *Biochem. J.*, 1980, **191**, 411.
18 P. N. Schatz, R. L. Mowery and E. R. Krausz, *Mol. Phys.*, 1978, **35**, 1537.
19 R. Hoffmann, *J. Chem. Phys.*, 1963, **39**, 1397.
20 J. H. Ammeter, H. B. Bürgi, J. C. Thibeault and R. Hoffmann, *J. Am. Chem. Soc.*, 1978, **100**, 3686.
21 Y. Zhang, M. A. Pavlosky, C. A. Brown, T. E. Westre, B. Hedman, K. O. Hodgson and E. I. Solomon, *J. Am. Chem. Soc.*, 1992, **114**, 9189.
22 D. G. Eglinton, Ph.D. Thesis, University of East Anglia, 1981.
23 R. J. Leatherbarrow, Grafit Version 3.0, Erithacus Software Ltd, Staines, 1992.

Received 22*nd March* 1993; *Paper* 3/01634J